

Numerical study of Kondo impurity models with strong potential scattering: Reverse Kondo effect and antiresonance

Annamária Kiss,^{1,2,*} Yoshio Kuramoto,³ and Shintaro Hoshino³

¹*Budapest University of Technology and Economics, Institute of Physics and Condensed Matter Research Group of the Hungarian Academy of Sciences, H-1521 Budapest, Hungary*

²*Research Institute for Solid State Physics and Optics, P.O. Box 49, H-1525 Budapest, Hungary*

³*Department of Physics, Tohoku University, Sendai, 980-8578, Japan*

(Received 22 June 2011; revised manuscript received 7 September 2011; published 2 November 2011)

Accurate numerical results are derived for transport properties of Kondo impurity systems with potential scattering and orbital degeneracy. Using the continuous-time quantum Monte Carlo (CT-QMC) method, static and dynamic physical quantities are derived in a wide temperature range across the Kondo temperature T_K . With strong potential scattering, the resistivity tends to decrease with decreasing temperature, in contrast to the ordinary Kondo effect. Correspondingly, the quasiparticle density of states obtains the antiresonance around the Fermi level. Thermopower also shows characteristic deviation from the standard Kondo behavior, while magnetic susceptibility follows the universal temperature dependence even with strong potential scattering. It is found that the t -matrix in the presence of potential scattering is not a relevant quantity for the Friedel sum rule, for which a proper limit of the f -electron Green's function is introduced. The optical theorem is also discussed in the context of Kondo impurity models with potential scattering. It is shown that optical theorem holds not only in the Fermi-liquid range but also for large energies, and therefore is less restrictive than the Friedel sum rule.

DOI: [10.1103/PhysRevB.84.174402](https://doi.org/10.1103/PhysRevB.84.174402)

PACS number(s): 72.10.Fk

I. INTRODUCTION

A single magnetic impurity embedded into the sea of conduction electrons shows Kondo effect. Although this problem has been almost continuously studied during the last 40 years, dynamic and magnetic properties of the Kondo and related models still attract great interest in condensed matter physics. Much less attention is paid to anomalous *decrease* of resistivity with lowering temperature since such decrease can be caused by many different mechanisms. The first attention to this problem is traced back to the 60s, when resistivity of dilute Fe and Cu alloys in Rh matrix revealed a new type of anomaly at low temperatures.¹ Namely, it was observed that resistivity decreases with decreasing temperature in these compounds. Obviously a ferromagnetic exchange interaction of a localized spin with conduction electrons is the first candidate. In fact, later study on dilute Gd and Nd impurities in some La alloys such as LaAl₂,² and LaSn₃³ explained the resistivity anomaly in terms of the ferromagnetic exchange model,⁴ and was referred to as the “reverse Kondo effect.”

In dilute Rh alloys, however, the measured susceptibility indicates antiferromagnetic exchange interaction in these materials in contrast with the behavior of the resistivity. As an alternative interpretation, Fischer found that a strong potential scattering can change the sign of the Kondo logarithmic term in the resistivity.⁵ The treatment has been much extended and deepened by Kondo,⁶ who uses the scattering phase shift δ_v of conduction electrons at the Fermi surface. The strength v of the potential scattering is related to the phase shift by $\tan \delta_v = -\pi v \rho_c$ where ρ_c is the density of states at the Fermi surface. The leading logarithmic term in the electric resistivity changes sign when $|\delta_v|$ exceeds $\pi/4$, defining a critical value for the potential scattering as $v_{cr} \equiv 1/(\pi \rho_c)$. The range $|v| > v_{cr}$ is called the reverse Kondo range. In this range the resistivity decreases with decreasing temperature as a consequence of the strong potential scattering. Regarding

thermodynamic properties, on the other hand, Kondo revealed that they show universal behavior even in the reverse Kondo range with strong potential scattering.

Since ordinary scattering events are always present in real systems, the Kondo problem with strong potential scattering might have relevance also in other compounds that show the Kondo effect. For example, the question of relevance of ordinary scattering in URu₂Si₂ arises, because (i) recent STM experiments have found that the density of electronic states shows Fano lineshape (i.e., antiresonance) in the normal phase,⁷ and (ii) in the dilute system U_xTh_{1-x}Ru₂Si₂ the resistivity decreases with decreasing temperature.⁸

In this paper we study the effect of strong potential scattering on physical properties of the Kondo impurity. In order to deal with the Kondo effect beyond the weak coupling regime, the continuous-time quantum Monte Carlo (CT-QMC) method is employed.⁹⁻¹² In the CT-QMC simulation it is most convenient to take the N -component Coqblin-Schrieffer (CS) model^{10,13} with potential scattering. The Hamiltonian is given by

$$\mathcal{H}_{CS}[v_{CS}] = \sum_{\mathbf{k}m} \varepsilon_{\mathbf{k}} c_{\mathbf{k}m}^\dagger c_{\mathbf{k}m} + \sum_{mm'} (J f_m^\dagger f_{m'} + v_{CS} \delta_{mm'}) c_{m'}^\dagger c_m, \quad (1)$$

where $c_{\mathbf{k}m}^\dagger$ and f_m^\dagger are creation operators of conduction and localized electrons, respectively, at the impurity site with SU(N) index $m = 1, \dots, N$. The constraint $\sum_m f_m^\dagger f_m = 1$ is imposed, which removes the charge degrees of freedom. The annihilation operator c_m in the Wannier representation is related to $c_{\mathbf{k}m}$ by $c_m = N_0^{-1/2} \sum_{\mathbf{k}} c_{\mathbf{k}m}$ with N_0 being the number of lattice sites. We observe the relation,

$$\sum_{mm'} f_m^\dagger f_{m'} c_{m'}^\dagger c_m = \sum_{mm'} \tilde{X}_{mm'} c_{m'}^\dagger c_m + \frac{1}{N} n_c \Rightarrow 2\mathbf{S}_f \cdot \mathbf{s}_c + \frac{1}{2} n_c, \quad (2)$$

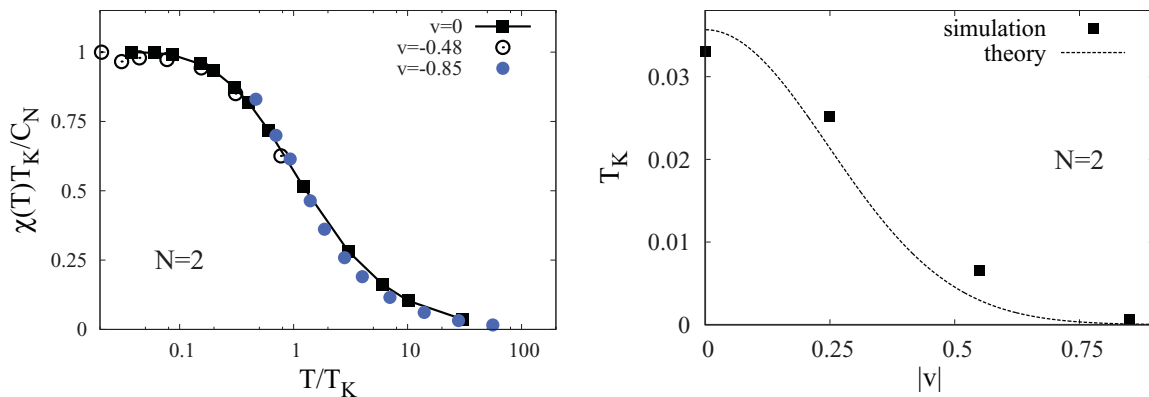


FIG. 1. (Color online) (Left) Temperature dependence of the static susceptibility for the Kondo model ($N = 2$) with potential scattering. Potential scattering v and exchange J are chosen as $v = 0, -0.85$ ($J = 0.3$), and $v = -0.48$ ($J = 0.44$). (Right) Kondo temperature for several values of potential scattering obtained in simulation. The theoretical result $T_K = D \exp[1/(2\rho\tilde{J})]$ is also shown as a dashed line.

where $\tilde{X}_{mm'} \equiv f_m^\dagger f_{m'} - \delta_{mm'}/N$ are $SU(N)$ generators, and s_c and n_c are spin and charge density operators of conduction electrons at the impurity site. The $SU(N)$ Kondo Hamiltonian $\mathcal{H}_K[v]$ with potential scattering v is introduced by the relation,

$$\mathcal{H}_{CS}[v_{CS}] = \mathcal{H}_K[v = v_{CS} + J/N], \quad (3)$$

in view of Eq. (2). Some typical cases of the model given by Hamiltonian (1) are as follows:

- (i) The conventional CS model with $v_{CS} = 0$, or $v = J/N$;
- (ii) The $SU(N)$ Kondo model with $v = 0$, or $v_{CS} = -J/N$;
- (iii) The reverse Kondo range with $|v| > v_{cr} = 1/(\pi\rho_c)$.

On the basis of accurate numerical results for strong potential scattering, we investigate the reverse Kondo range in detail. Furthermore, properties are studied by changing the orbital degeneracy N for the $SU(N)$ Kondo model. This paper is organized as follows. In Sec. II numerical results for the magnetic susceptibility are presented. The characteristics of the impurity t -matrix are discussed in Sec. III. Furthermore, numerical results are given for transport properties. Section IV is devoted to discussion of quasiparticle properties including the Friedel sum rule and optical theorem. The summary of this paper will be given in Sec. V.

II. MAGNETIC SUSCEPTIBILITY AND UNIVERSALITY

The static susceptibility is obtained from the imaginary time data by integration as

$$\chi(T) = \int_0^\beta d\tau \chi(\tau) = \int_0^\beta d\tau \langle T_\tau M^H(\tau) M \rangle, \quad (4)$$

where the dipole moment M is given by $M = \sum_\alpha m_\alpha f_\alpha^\dagger f_\alpha$ with coefficients m_α chosen as $\sum_\alpha m_\alpha = 0$, and the superscript H denotes the Heisenberg picture.¹⁰ We use a constant density of states for the conduction electrons in the simulation as

$$\rho_c(\varepsilon) = \rho_0 \Theta(D - |\varepsilon|), \quad (5)$$

where $\rho_0 = 1/(2D)$ with $D = 1$ as a unit of energy. In the numerical study, we determine the Kondo temperature from the low-temperature static susceptibility as

$$T_K^{-1} = \chi(T \rightarrow 0)/C_N, \quad (6)$$

where C_N is the Curie constant. The critical strength v_{cr} is given by $v_{cr} = 1/(\pi\rho_0) = 0.637$.

From now on until Sec. IIIB we confine ourselves to the case of orbital degeneracy $N = 2$, which corresponds to the original Kondo model. The left part of Fig. 1 shows $\chi(T)$ of the Kondo model with several values of the potential scattering v . We observe in Fig. 1 that the susceptibility shows universal behavior as a function of T/T_K independent of the value of the potential scattering. Note that the data with $v = -0.85$ as shown by blue symbols are in the reverse Kondo range with δ_v being larger than $\pi/4$. Even in this case, the temperature evolution of the magnetic susceptibility shows the universal behavior.

In order to understand the behavior of the magnetic susceptibility shown in Fig. 1, we recall the result obtained by Kondo.⁶ He showed in Ref. 6 that the effect of ordinary scattering is entirely absorbed into an effective exchange interaction $\tilde{J} = J \cos^2 \delta_v$ which remains antiferromagnetic for all values of the potential scattering. Therefore, thermodynamic quantities behave universally even for large values of v . Correspondingly, the low-temperature energy scale is characterized by temperature $T_K = D \exp[1/(2\rho_c \tilde{J})]$ associated with the effective exchange interaction \tilde{J} . The right part of Fig. 1 shows the Kondo temperature T_K for different values of v . The result $T_K = D \exp[1/(2\rho_c \tilde{J})]$ obtained by Kondo⁶ is also shown for comparison.

III. TRANSPORT COEFFICIENTS

A. t -matrix and Fano lineshape

We have already shown in Eq. (2) that the Kondo and CS Hamiltonians are related to each other through a potential scattering term. In the simulation for the CS model, instead of the bare Green's function g , another Green's function g_{CS} is used that absorbs the potential scattering v_{CS} :

$$g_{CS} = g/(1 - v_{CS}g), \quad (7)$$

where $g(z) = \sum_{\mathbf{k}} (z - \varepsilon_{\mathbf{k}})^{-1}$. Then the simulation gives the renormalized Green's function G of conduction electrons. We

introduce a quantity t_{CS} by the relation,

$$G = g_{CS} + g_{CS}t_{CS}g_{CS}. \quad (8)$$

On the other hand, the t -matrix t of conduction electrons is defined by the relation,

$$G = g + gtg. \quad (9)$$

By comparing Eqs. (8) and (9), we obtain t from t_{CS} by the relation,

$$t = v_{CS}/(1 - v_{CS}g) + t_{CS}/(1 - v_{CS}g)^2. \quad (10)$$

In the special case of $v = v_{CS} + J/2 = 0$, we recover Eq. (33) in Ref. 10.

In the CT-QMC simulation, the t -matrix is derived in the imaginary-time domain. In order to obtain properties in the real energy domain, analytic continuation of the numerical data is done by using Padé approximation.¹⁴ The data obtained by CT-QMC are so accurate that the Padé approximation works well to perform the analytic continuation. In the approximation we construct the rational function that provides approximate values at an arbitrary real energy point up to degree $\sim 10^3$. We checked the accuracy of the t -matrix obtained in the real energy domain by comparing the lines derived for the different channels (e.g., for spin up and down when $N = 2$). We note that analytic continuation may cause a problem in CT-QMC when the spectrum is complicated since the extrapolation does not work well in this case.

Figure 2 shows the energy dependence of the impurity t -matrix for three different values of the potential scattering at various temperatures. To simplify the notation, we take the convention in this paper that energy including an infinitesimal imaginary part, $\varepsilon + i\delta$, is simply written as ε . The left panel of Fig. 2 with the value $v = 0.15$ corresponds to the CS model, the center panel with $v = 0$ to the ordinary single-channel Kondo model, while the right panel corresponds to a strong potential scattering $|v| > v_{cr} = 0.637$. In the case of the ordinary single-channel Kondo model the spectrum is symmetric with respect to the Fermi energy, because the model has particle-hole symmetry in this limit. Increasing the value of the potential scattering, the Kondo peak first moves to higher frequencies above the Fermi energy. Finally, for strong

potential scattering the spectrum becomes highly asymmetric showing an antiresonance around the Fermi level.

Interpretation of the asymmetric spectrum with large $|v|$ can be provided in terms of the Anderson model, which reproduces the Kondo model in the limit of deep local electron level ε_f and large Coulomb repulsion U as compared with hybridization V . Namely we take the limits ($\varepsilon_f \rightarrow -\infty$, $\varepsilon_f + U \rightarrow \infty$, and $V^2 \rightarrow \infty$, keeping the ratio $J = -2V^2/\varepsilon_f$ finite), which we call the Schrieffer-Wolff limit. Now we construct the f -electron Green's function G_{fv} of the Anderson model in the presence of potential scattering. Let us first consider the pure case $v = 0$. Introducing the irreducible part $F(z)$, we obtain the Green's function,

$$G_f(z) = F(z)[1 + V^2g(z)G_f(z)]. \quad (11)$$

In the presence of potential scattering, the f -electron Green's function $G_{fv}(z)$ satisfies the following relation:

$$G_{fv}(z) = F_v(z)[1 + V^2g_v(z)G_{fv}(z)], \quad (12)$$

where $g_v(z) = g(z)/[1 - vg(z)]$.

The t -matrix for the Kondo model is given by

$$t(z) = \frac{v + V^2F_v(z)}{1 - g(z)[v + V^2F_v(z)]} = t_v(z) + \frac{V^2G_{fv}(z)}{[1 - vg(z)]^2}, \quad (13)$$

where $t_v = v/(1 - vg)$. It is clear from Eq. (13) that the t -matrix reduces to

$$t(z) \rightarrow V^2G_f(z), \quad (14)$$

in the limit of $v = 0$ as we expect. We derive from Eq. (13),

$$V^2G_{fv} = (1 - vg)^2(t - t_v), \quad (15)$$

which remains finite in the Schrieffer-Wolff limit.

As the simplest case, let us consider the noninteracting Anderson model with $U = 0$. Then we obtain $F(\varepsilon) = 1/(\varepsilon + i\delta - \varepsilon_f) \equiv 1/\xi$, which is not affected by potential scattering. The imaginary part of the f -electron Green's function is given by

$$-\text{Im} G_{fv}(\varepsilon) = \frac{1}{V^2} \cdot \frac{\pi\rho_0(v + V^2/\xi)^2}{1 + \pi^2\rho_0^2(v + V^2/\xi)^2}. \quad (16)$$

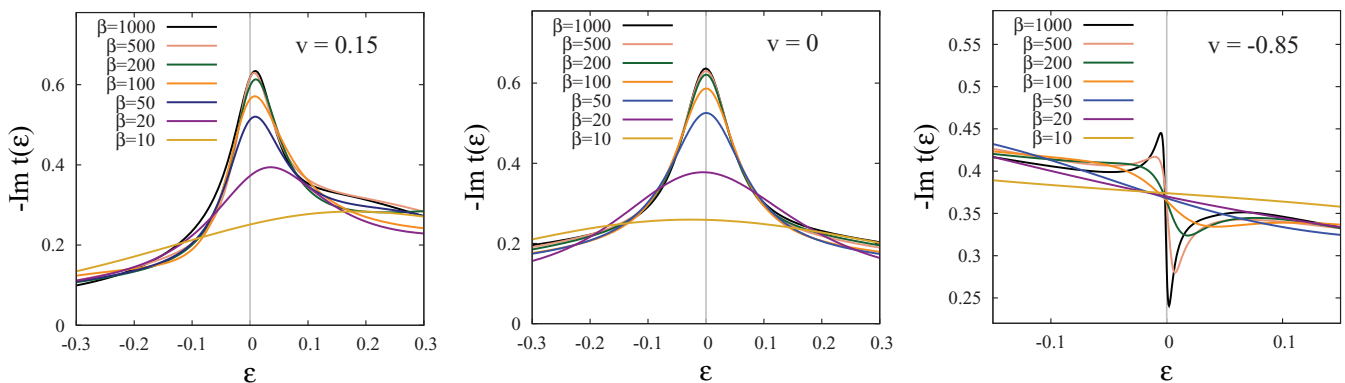


FIG. 2. (Color online) Energy dependence of $-\text{Im} t(\varepsilon)$ for the Kondo model ($N = 2$) with potential scattering with $J = 0.3$. Potential scattering terms are chosen as $v = 0.15$ (left), $v = 0$ (center), and $v = -0.85$ (right). Values $v = 0.15$ and $v = 0$ correspond to the CS and ordinary Kondo models, respectively.

Under the transformation $v \rightarrow -v$, the imaginary part of the Green's function given in Eq. (16) remains the same if we put $\varepsilon - \varepsilon_f \rightarrow \varepsilon_f - \varepsilon$. Physically it means that the antiresonance is reflected with respect to the energy ε_f when v changes sign. Expression (16) can be put into the standard form of the Fano lineshape.¹⁵ Introducing the dimensionless parameter q by $1/q \equiv \pi v \rho_0$, we rearrange the terms as follows:

$$-\frac{V^2}{v} \text{Im} G_{fv}(\varepsilon) = \frac{1}{q + 1/q} \cdot \frac{(x + q)^2}{x^2 + 1}, \quad (17)$$

where x is the dimensionless energy defined by

$$x = \frac{v}{V^2} \left(q + \frac{1}{q} \right) \xi + \frac{1}{q}. \quad (18)$$

The degree of asymmetry is determined by the parameter q that is independent of hybridization.

Expression (16) describes the characteristics of the simulation results for $t(\varepsilon)$ shown in Fig. 2, provided we put $\varepsilon_f \sim 0$. We note that $V^2 G_{fv}(z)$ is not the same as the t -matrix $t(z)$ of the Kondo model as shown in Eq. (13). However, the characteristic lineshape comes almost from $V^2 G_{fv}(z)$ since $t_v(z)$ and $1 - vg(z)$ do not have strong dependence on z . The asymmetric spectrum for strong potential scattering has interesting consequences with respect to transport properties such as the resistivity or thermopower. This problem is discussed in the next subsection.

B. Relaxation time and transport coefficients

We rely on the Boltzmann equation approach¹⁶ to derive transport coefficients. Then the relaxation time $\tau(\varepsilon)$ is related to the t -matrix as¹⁷

$$\tau(\varepsilon)^{-1} = -2\text{Im} t(\varepsilon). \quad (19)$$

Let us introduce the integrals:¹⁸

$$L_n = \int_{-\infty}^{\infty} d\varepsilon \left(-\frac{\partial f(\varepsilon)}{\partial \varepsilon} \right) \tau(\varepsilon) \varepsilon^n, \quad (20)$$

in terms of which the conductivity σ , thermopower S , and thermal conductivity κ are expressed as

$$\sigma(T) = L_0, \quad (21)$$

$$S(T) = -\frac{1}{T} \frac{L_1}{L_0}, \quad (22)$$

$$\kappa(T) = \frac{1}{T} \left(L_2 - \frac{L_1^2}{L_0} \right). \quad (23)$$

The integrals in Eq. (20) are evaluated numerically with the CT-QMC data for the t -matrix.

Although many theoretical attempts were made to derive the transport properties for the Kondo problem analytically in the whole temperature range, none of these attempts was successful. However, there are correct results in limiting cases such as Hamman's formula¹⁹ for $T \gg T_K$, Fermi-liquid results²⁰ for $T \ll T_K$, or expressions for large values of the orbital degeneracy N .²¹ In the local Fermi-liquid range at low temperatures, the resistivity $R(T)$ shows the following temperature dependence:

$$R(T)/R(0) = 1 - \alpha (T/T_K)^2, \quad (24)$$

where we have used the relation $R(T)/R(0) = \sigma(0)/\sigma(T)$, and α is a numerical coefficient. For large values of the orbital degeneracy N , the $1/N$ expansion gives the coefficient α in Eq. (24) as²¹

$$\alpha = \pi^2 \left(1 - \frac{8}{3N} \right). \quad (25)$$

This limiting result gives checkpoint of our numerical calculations.

C. Behavior under varying potential scattering

Figure 3 shows the temperature dependence of the normalized electric resistivity for the Kondo model ($N = 2$) across the Kondo temperature. For $|v| < v_{\text{cr}} = 0.637$, the resistivity follows universal behavior as a function of T/T_K . As the potential scattering increases beyond the critical value, the resistivity still follows the universal behavior in the Fermi-liquid range $T \ll T_K$. As temperature increases, the resistivity starts to deviate from the universal curve around the Kondo temperature $T \sim T_K$, and shows increasing behavior as the temperature is further increased. In the temperature range $T \gg T_K$, we find that the resistivity for strong potential scattering can be described well with Kondo's formula⁶ shown by the dashed line in Fig. 3. However, Kondo's formula cannot describe the properties for $T \leq T_K$. Based on the numerical results for $T \ll T_K$, the coefficient α in Eq. (24) appears to be independent of v .

The left panel of Fig. 4 shows the temperature dependence of normalized thermal conductivity for the Kondo model ($N = 2$) under varying the potential scattering. The thermal conductivity also follows the universal behavior even for large values of the potential scattering in the temperature range $T \ll T_K$. Namely we obtain

$$\frac{\kappa(T)}{T} \bigg/ \left(\frac{\kappa(T)}{T} \right)_0 = 1 + \gamma \left(\frac{T}{T_K} \right)^2, \quad (26)$$

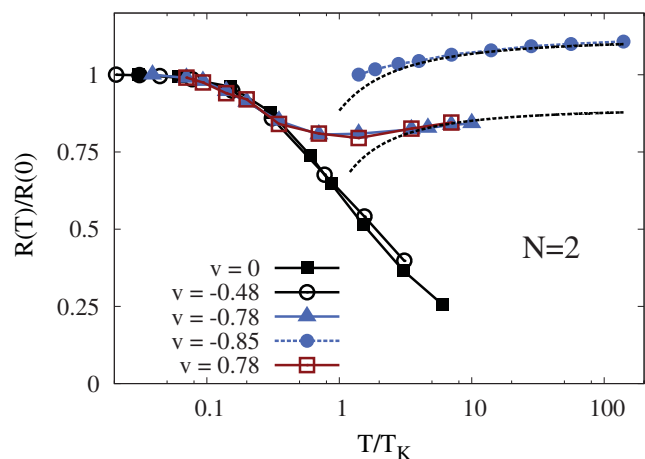


FIG. 3. (Color online) Temperature dependence of the normalized resistivity for the Kondo model ($N = 2$) with potential scattering. Potential scattering v and exchange J are chosen as $v = 0, -0.85$ ($J = 0.3$), and $v = 0.78, -0.48, -0.78$ ($J = 0.44$). The dashed line corresponds to Kondo's result for the resistivity given in Ref. 6.

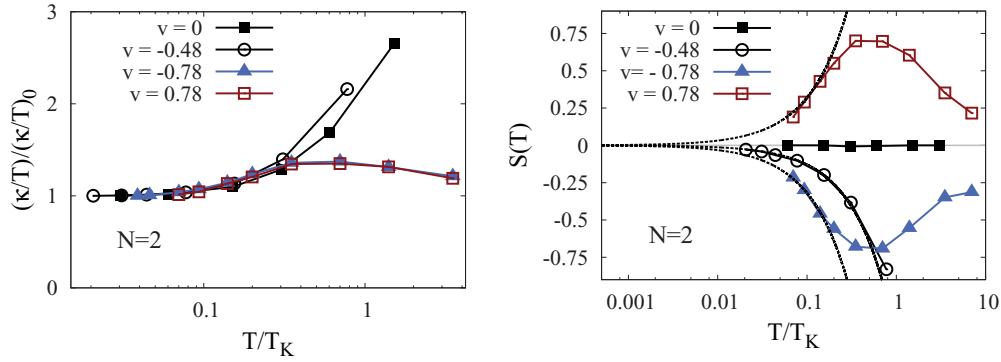


FIG. 4. (Color online) Temperature dependence of normalized thermal conductivity (left) and thermopower (right) for the Kondo model ($N = 2$) with potential scattering. Potential scattering v and exchange J are chosen as $v = 0$ ($J = 0.3$), and $v = 0.78, -0.48, -0.78$ ($J = 0.44$). The dashed line in the right panel corresponds to the Fermi-liquid behavior $S(T) \sim T$.

with γ being a numerical constant independent of v . Increasing further the temperature, thermal conductivity with large potential scattering highly deviates from the universal behavior. Namely, it decreases with increasing temperature for $T \gg T_K$.

The right panel of Fig. 4 shows the temperature dependence of thermopower for the Kondo model ($N = 2$) under varying potential scattering. The asymmetry of the impurity t -matrix is most reflected in the behavior of thermopower. This is clear if we regard explicitly the expression for the integral L_1 given in Eq. (20):

$$L_1 = \frac{1}{2} \int_{-\infty}^{\infty} d\varepsilon \frac{f'(\varepsilon) \varepsilon}{\text{Im} t(\varepsilon)}. \quad (27)$$

Because of the factor ε in the numerator, the thermopower measures the asymmetry in the energy dependence of $\text{Im} t(\varepsilon)$. Since the spectra is completely symmetric in the case of the ordinary Kondo model ($v = 0$), the thermopower vanishes in this case as we obtain in the simulation (see Fig. 4). On the other hand, the thermopower acquires strong temperature dependence when the potential scattering term is increased from $v = 0$. The thermopower in the simulation shows Fermi-liquid property,

$$S(T) = \beta \left(\frac{T}{T_K} \right), \quad (28)$$

for $T \ll T_K$. The coefficient β is negative for $v < 0$, while it is positive for $v > 0$. The different sign of β can be simply understood if we recall that the asymmetry in the lineshape of $\text{Im} t(\varepsilon)$ around the Fermi level is reversed against the sign change $v \rightarrow -v$. Thus, the integrals given in Eq. (20) have the properties $L_0(L_2) \rightarrow L_0(L_2)$ and $L_1 \rightarrow -L_1$ under the sign change. Namely, the electric resistivity $R(T)$ and thermal conductivity $\kappa(T)$ remain the same under $v \rightarrow -v$, while the thermopower changes sign as $S(T) \rightarrow -S(T)$. We have indeed obtained these behaviors in the simulation as it can be seen in Figs. 3 and 4.

D. Behavior under varying orbital degeneracy N

Let us now study the effect of orbital degeneracy. The left panel of Fig. 5 shows the temperature dependence of the normalized electric resistivity for large values of the orbital degeneracy for the $SU(N)$ Kondo model with the condition $v = J/N$, which corresponds to the case of the CS model, across the Kondo temperature. We observe again the universal behavior for a given value of the orbital degeneracy N . In contrast to the behavior of the magnetic susceptibility, the resistivity decreases monotonically as the temperature is increased even for large N . In order to understand this feature, we assume that the t -matrix at low temperature is determined

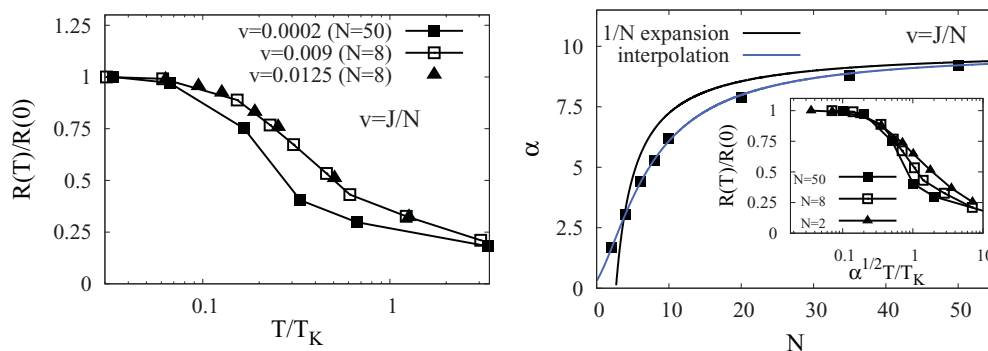


FIG. 5. (Color online) (Left) Temperature dependence of the normalized resistivity for the $SU(N)$ Kondo model with the condition $v = J/N$ for orbital degeneracies $N = 8$ with $J = 0.075, 0.1$ and $N = 50$ with $J = 0.0115$. (Right) Orbital degeneracy N dependence of the coefficient α of the T^2 term in the low-temperature resistivity defined in Eq. (24). The inset shows the scaling behavior of the resistivity for different orbital degeneracies including α .

by the quasiparticle density of states, which is approximately given by the effective Anderson model. Namely we assume

$$t(z) = V^2 G_f(z), \quad (29)$$

where V is the effective hybridization and G_f is the Green's function of the local electron in the effective Anderson model. Then the Sommerfeld expansion of the conductivity leads to

$$\sigma(T) \sim \int_{-\infty}^{\infty} \frac{1}{\rho_f(\varepsilon)} \left(-\frac{\partial f(\varepsilon)}{\partial \varepsilon} \right) d\varepsilon = \frac{1}{\rho_f(0)} \left(1 + \frac{\pi^2}{6} (k_B T)^2 \times \left[2 \left(\frac{\rho_f'(0)}{\rho_f(0)} \right)^2 - \frac{\rho_f''(0)}{\rho_f(0)} \right] + \mathcal{O}(T^4) \right), \quad (30)$$

where

$$\rho_f(\varepsilon) = -\pi^{-1} \text{Im} G_f(\varepsilon). \quad (31)$$

We obtain the resistivity $R(T) = \sigma(T)^{-1}$ from Eq. (30). Using the quasiparticle density of states for the noninteracting Anderson model with $v = 0$, we obtain

$$R(T) \sim \rho_f(0) \left[1 - \frac{\pi^2}{3} (k_B T)^2 \frac{1}{(\eta^2 + \Delta^2)} + \mathcal{O}(T^4) \right], \quad (32)$$

where η and Δ are the shift and the width of the resonance peak appearing in $\rho_f(\varepsilon)$ at low temperatures. Irrespective of the magnitude of parameters η and Δ , the coefficient of the T^2 term in the low- T resistivity is always negative. Hence $R(T)$ given by Eq. (32) decreases as temperature increases for any value of N . Namely, the quasiparticle picture is consistent with the monotonous change obtained in the simulation.

The resistivity obtained numerically has T^2 temperature dependence at low temperatures, which is expressed generally in Eq. (24). The right panel of Fig. 5 shows the coefficient α of the T^2 term for several values of the orbital degeneracy N obtained in the simulation. The result of $1/N$ expansion²¹ given in Eq. (25) is also shown in the figure. We find that the numerical data coincide with the $1/N$ expansion result for large values of the degeneracy N . Thus, our CT-QMC simulation has produced accurate numerical results for large values of orbital degeneracies $N \rightarrow \infty$, which might be difficult in the case of other numerical techniques. For small values of degeneracy N , the coefficient α shows linear- N dependence in our simulation.

Now we fit the simulated N dependence of α by a rational function as $\alpha(N) = F_1^{(l)}(N)/F_2^{(m)}(N)$, where $F_k^{(l)} = c_{k0} + c_{k1}N + \dots + c_{kl}N^l$. We find that the minimal function which can give a good fit to the numerical data has the form,

$$\alpha(N) = \frac{c_{10} + c_{11}N + c_{12}N^2}{1 + c_{21}N + c_{22}N^2}. \quad (33)$$

The limiting cases $N \rightarrow 0$ and $N \rightarrow \infty$ are obtained from the formula (33) as

$$\alpha(N \rightarrow 0) \sim c_{10} + (c_{11} - c_{10}c_{21})N, \quad (34)$$

and

$$\alpha(N \rightarrow \infty) \sim \frac{c_{12}}{c_{22}} \left[1 - \frac{1}{N} \left(\frac{c_{11}}{c_{12}} - \frac{c_{21}}{c_{22}} \right) \right]. \quad (35)$$

Choosing the coefficients in Eq. (33) as $c_{10} = 0.3$; $c_{11} = 0.53$; $c_{12} = 0.17$; $c_{21} = 0.1$; $c_{22} = 0.0173$, the numerical data can be fitted well (see Fig. 5). The result of $1/N$ expansion²¹ given in Eq. (25) is also reproduced in the large- N range. In the inset of the right part of Fig. 5 we plot the normalized resistivity for different values of orbital degeneracy N as a function of $\alpha(N)^{1/2}T/T_K$. The results show the scaling behavior of the resistivity in the Fermi-liquid range. For $T \geq T_K$, the scaling property breaks down.

In Fig. 6, thermal conductivity κ and thermopower S are shown for the $SU(N)$ Kondo model with orbital degeneracy $N = 8$. The low- T behaviors of $\kappa(T)$ and $S(T)$ are consistent with the Fermi-liquid result given in Eqs. (26) and (28). As the temperature is further increased, the thermopower $S(T)$ has a peak, while the thermal conductivity $\kappa(T)$ monotonously increases. Both quantities show universal behavior as a function of T/T_K .

Note that the coefficient β for $S(T)$ has a positive sign for large N . This behavior is explained as follows. In a manner similar to Eq. (30), L_1 is given by

$$L_1(T) = \int_{-\infty}^{\infty} \frac{\varepsilon}{\rho_f(\varepsilon)} \left(-\frac{\partial f}{\partial \varepsilon} \right) = -\frac{2\pi^3}{3\Delta} \eta T^2. \quad (36)$$

Using the result for L_0 given by Eq. (32), we obtain $S(T)$ in the lowest order of T as

$$S(T) = \frac{2\pi^2}{3} \frac{\eta}{\eta^2 + \Delta^2} T = \beta T. \quad (37)$$

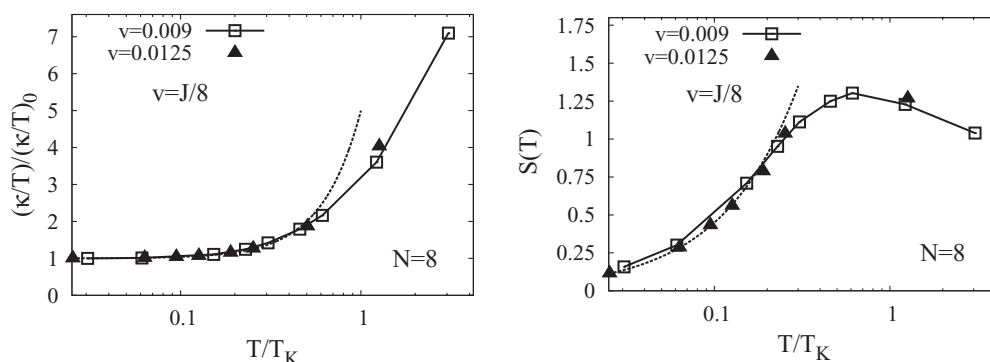


FIG. 6. Temperature dependence of normalized thermal conductivity (left) and thermopower (right) for the $SU(N)$ Kondo model with the condition $v = J/N$ for orbital degeneracy $N = 8$. Potential scattering terms are chosen as $v = 0.009$ ($J = 0.075$) and $v = 0.0125$ ($J = 0.1$). The dashed line corresponds to the Fermi-liquid behavior given in Eqs. (28) and (26).

Since $\eta \sim T_K > 0$ for large N , we obtain $\beta > 0$. On the other hand, we obtain $\eta = 0$ for the symmetric Anderson model with $N = 2$. In this case, the sign of β depends on the sign of v as it can be observed in Fig. 4.

IV. QUASIPARTICLE PROPERTIES

A. Friedel sum rule

At temperatures $T \ll T_K$, the conduction electrons screen the magnetic impurity and they together form a local singlet. In this range the ground state is a local Fermi liquid. The Friedel sum rule (FSR) relates the phase shift for scattering of the conduction electrons by the impurity to its charge. In the case of the Kondo model, the f -electron Green's function cannot be defined because there is no charge degree of freedom in this localized model since it is eliminated. Instead, the impurity t -matrix is used to describe the effect of exchange and potential scatterings. In Sec. III, we have related the t -matrix to the Green's function $G_{fv}(z)$ of localized electrons with potential scattering v . It is the quantity $G_{fv}(z)$ that is expected to keep the FRS in the presence of v .

The FSR reads¹⁷

$$V^2 G_f(0) = -\frac{i}{\pi \rho_0} \sin^2\left(\frac{\pi}{N}\right), \quad (38)$$

since the occupation number is unity in the Kondo model.

Figure 7 shows the Green's function $G_{fv}(0)$ obtained by simulation at finite temperatures. For small potential scattering the simulation results show good agreement with the expectation given in Eq. (38). As the value of v is increased, $\text{Re } V^2 G_{fv}(0)$ is still close to zero, but $-\text{Im } V^2 G_{fv}(0)$ highly deviates from the theoretical result. The reason for this deviation is the following. The theoretical result given in Eq. (38) is realized at $T = 0$, which is almost realized for $T \ll T_K$ in the simulation. As the value of the potential scattering is increased, however, the corresponding Kondo temperature $T_K = D e^{1/(2\rho\tilde{J})}$ rapidly decreases since the effective coupling \tilde{J} decreases rapidly.⁶ Therefore, we have to go to lower and lower temperatures in the simulation to achieve the condition $T \ll T_K$, which is not fulfilled in Fig. 7 for large values of v since the results are obtained for a fixed temperature value

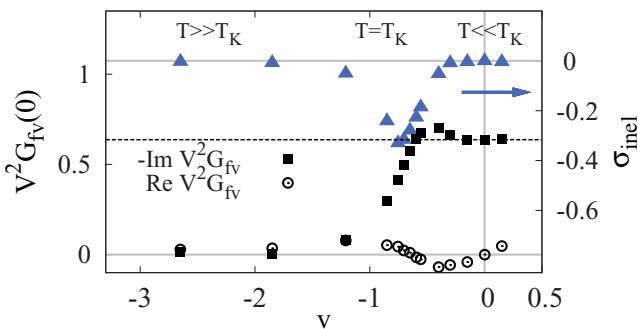


FIG. 7. (Color online) Imaginary and real parts of the Green's function G_{fv} expressed in Eq. (15) at the Fermi level as a function of potential scattering v together with the analytical result for $-\text{Im } V^2 G_{fv}(0)$ obtained from the FSR (dashed line). The figure also shows the inelastic scattering cross section σ_{inel} as blue triangles. The numerical data are obtained at temperature $\beta = 1/T = 1000$.

$\beta = 1/T = 1000$. In principle it is possible to go to lower temperatures in the simulation, but it becomes computationally harder.

B. Optical theorem

The optical theorem is less restrictive than the FSR since the former does not require the Fermi-liquid ground state. Optical theorem is related to the unitarity of the S matrix,²² and it follows when the scattering of the conduction electrons from the impurity is totally elastic at the Fermi level. Optical theorem was originally formulated for problems of scattering of a single particle. When the scattering event happens without energy loss (i.e., it is totally elastic), there is a relation between the square and the imaginary part of the t -matrix. To express this relation, the S matrix is decomposed as²³

$$S = 1 + iT, \quad (39)$$

where we write the matrix element of the t -matrix T as $\langle n|T|n' \rangle = 2\pi \delta(\varepsilon_n - \varepsilon_{n'}) \langle n|t|n' \rangle$. Here, a state $|n \rangle$ represents a single-particle state with momentum \mathbf{k} and spin σ as $|n \rangle = |\mathbf{k}\sigma \rangle$. After some manipulations we obtain from relation (39) that

$$\langle k|SS^\dagger|k \rangle - 1 = 2\pi \left[2\pi \sum_n \delta(\varepsilon_k - \varepsilon_n) \langle n|t|k \rangle^2 + 2\text{Im} \langle k|t|k \rangle \right]. \quad (40)$$

The first term of Eq. (40) in the right-hand side is related to the elastic scattering cross section σ_{el} , while the second term to the total scattering cross section σ_{total} as^{23,24}

$$\sigma_{\text{el}} = -2\pi \sum_n \delta(\varepsilon_k - \varepsilon_n) \langle n|t|k \rangle^2, \quad (41)$$

$$\sigma_{\text{total}} = 2\text{Im} \langle k|t|k \rangle. \quad (42)$$

The inelastic scattering cross section σ_{inel} is the difference of σ_{total} and σ_{el} as

$$\sigma_{\text{inel}} = \sigma_{\text{total}} - \sigma_{\text{el}}. \quad (43)$$

For scattering only in the s channel and assuming spin conservation, the inelastic cross section is expressed as²⁴

$$\begin{aligned} \sigma_{\text{inel}}(\omega) &= (|s(\omega)|^2 - 1)/(2\pi) = 2\text{Im} t(\omega) + 2\pi \rho_0 |t(\omega)|^2 \\ &= 2\pi \rho_0 \left[\frac{1}{\pi \rho_0} \text{Im} t(\omega) + |t(\omega)|^2 \right], \end{aligned} \quad (44)$$

where s and t are eigenvalues of the S matrix and t -matrix, respectively.

The eigenvalues s of the S matrix lie within the complex unit circle. The scattering is completely elastic (i.e., $\sigma_{\text{inel}} = 0$) when the unitary condition $S S^\dagger = 1$ is satisfied, which means $|s|^2 = 1$. In this case we have the relation,

$$|t|^2 = -\frac{1}{\pi \rho_0} \text{Im} t, \quad (45)$$

from Eq. (44).

The problem is formulated so far for single-particle scattering, but it is more general and can be applied for many-particle problems as well such as the single-channel

Kondo model. It is the most easily understood in the limit of $\varepsilon \rightarrow \infty$, when the magnetic impurity is completely decoupled from the conduction electrons. In this case the conduction electrons scatter without energy loss, and the optical theorem is held. Although the t -matrix is complicated and contains many scattering events at low temperatures, strictly in the limit of $\varepsilon \rightarrow 0$ the optical theorem holds again. If we express the t -matrix as

$$t = |t|e^{i\theta}, \quad (46)$$

where θ is the phase of the t -matrix t . Equation (45) gives

$$-\text{Im } t(\varepsilon) = \frac{\sin^2 \theta}{\pi \rho_0} \quad (47)$$

for the Kondo model with energy not only $\varepsilon = 0$ but also $\varepsilon \rightarrow \infty$. Namely, relation (47) is satisfied in the case when the scattering is totally elastic. In the case of the ordinary single-channel Kondo model ($v = 0$), $\theta = -\pi/2$ at the Fermi energy, so from Eq. (47) we recover the FSR,

$$-\text{Im } t(0) = \frac{1}{\pi \rho_0}. \quad (48)$$

Let us discuss the optical theorem in the context of our numerical data. Figure 7 shows the obtained inelastic scattering cross section σ_{inel} as a function of potential scattering. Note that σ_{inel} shows nonmonotonous behavior as a function of v . Namely, σ_{inel} is almost zero for small values of the potential scattering, but becomes nonzero as $|v|$ is increased. With further increase of $|v|$, however, σ_{inel} approaches to zero again. Since T_K decreases as the potential scattering increases, in the large- v range the condition $T \gg T_K$ is satisfied at $T = 10^{-3}$ used in the simulation. On the other hand, in the small- v range we have the condition $T \ll T_K$ with the same value: $T = 10^{-3}$. It is confirmed in the simulation that the optical theorem holds both at $T \ll T_K$ and $T \gg T_K$, but not for $T \sim T_K$. This happens because the ranges $T \ll T_K$ and $T \gg T_K$ correspond to the limits $\varepsilon/T_K \ll 1$ and $\varepsilon/T_K \gg 1$, respectively, where expression (47) is satisfied as explained above.

V. SUMMARY

In this paper we have studied Kondo impurity models with potential scattering and orbital degeneracy by using the CT-QMC numerical technique. We have derived accurate numerical results for the impurity t -matrix, thermal, and transport properties in a wide temperature range across the Kondo temperature T_K . Properties in the reverse Kondo range have been investigated in detail. The results shown in this paper are numerically exact since CT-QMC does not use any approximation. We have explicitly demonstrated that the CT-QMC simulation technique gives numerically exact results for large values of the orbital degeneracy N , which might be difficult to achieve in the case of other numerical techniques.

For large values of the potential scattering, nontrivial physics appears even in the impurity problem. Namely, the resistivity shows an anomalous increase with increasing temperature in contrast to the ordinary Kondo effect. This unusual behavior is caused by an antiresonance developing around the Fermi energy in the quasiparticle density of states as the value of the potential scattering is increased. This

antiresonance does not influence the universal behavior of the magnetic susceptibility. However, the sign of the Kondo logarithmic term changes in the resistivity when the potential scattering exceeds a critical value (i.e., in the reverse Kondo range), which causes the resistivity decrease with decreasing temperature.

We have studied the effect of strong potential scattering on thermal and transport properties of the Kondo impurity, and obtained that (i) the magnetic susceptibility follows the universal temperature dependence even with strong potential scattering; (ii) the resistivity also follows the universal temperature dependence for small values of the potential scattering; (iii) when the potential scattering exceeds a critical value, the resistivity still shows universal behavior in the Fermi-liquid range, but starts to deviate from the universal curve around the Kondo temperature, and increases as the temperature is further increased; (iv) the obtained temperature dependence of the resistivity for $T \gg T_K$ in the reverse Kondo range agrees quantitatively with Kondo's theoretical result; (v) the thermal conductivity also shows universal behavior in the Fermi-liquid range, but highly deviates from the universal curve for $T \gg T_K$ in the reverse Kondo range; (vi) the asymmetry of the t -matrix developing with increasing value of the potential scattering is most reflected in the temperature dependence of the thermopower; and (vii) the sign of the thermopower depends on the sign of the potential scattering.

In addition to the study of thermal and transport properties, we have discussed the Friedel sum rule and optical theorem as well. We have shown that the t -matrix of the Kondo model in the presence of potential scattering is not the relevant quantity for the Friedel sum rule. Instead, the Friedel sum rule is satisfied with a proper limit of the f -electron Green's function. We have demonstrated that the optical theorem is less restrictive than the Friedel sum rule, because the former holds not only in the Fermi-liquid range, but for large energies as well.

Finally we mention an interesting question of whether the behavior found for strong potential scattering has relevance in real systems. Note that recent STM experiments on URu_2Si_2 have found that the density of states shows Fano lineshape in the normal phase, and in the dilute system $\text{U}_x\text{Th}_{1-x}\text{Ru}_2\text{Si}_2$ the resistivity decreases with decreasing temperature. Since some important aspect of the U ion with the non-Kramers configuration $5f^2$ may not be described by a localized spin with $S = 1/2$, account of the strong potential scattering in more realistic models is desirable. We hope that our results in this paper will stimulate further study concerning the Fano lineshape and other aspects, which reflect interplay of the Kondo effect and potential scattering.

ACKNOWLEDGMENTS

The authors are grateful to Dr. J. Otsuki for his guidance on the details of the CT-QMC simulation technique, and also for useful discussions. A.K. acknowledges the Magyar Programme and the EGT Norway Grants, and also financial support from the European Union Seventh Framework Programme through the Marie Curie Grant No. PIRG-GA-2010-276834.

*akiss@szfki.hu

- ¹B. R. Coles, *Phys. Lett.* **8**, 243 (1964).
²W. Lieke, J. H. Moeser, and F. Steglich, *Z. Physik B* **30**, 155 (1978).
³W. Schmid, E. Umlauf, F. Steglich, and P. Thalmeier, *Solid State Commun.* **35**, 325 (1980).
⁴W. Lieke, F. Steglich, K. Rander, and H. Keiter, *Phys. Rev. B* **20**, 2129 (1979).
⁵K. Fischer, *Phys. Rev.* **158**, 613 (1967).
⁶J. Kondo, *Phys. Rev.* **169**, 437 (1968).
⁷A. R. Schmidt, M. H. Hamidian, P. Wahl, F. Meier, A. V. Balatsky, J. D. Garrett, T. J. Williams, G. M. Luke, and J. C. Davis, *Nature (London)* **465**, 570 (2010).
⁸H. Amitsuka and T. Sakakibara, *J. Phys. Soc. Jpn.* **63**, 736 (1994).
⁹E. Gull, A. J. Millis, A. I. Lichtenstein, A. N. Rubtsov, M. Troyer, and P. Werner, *Rev. Mod. Phys.* **83**, 349 (2011).
¹⁰J. Otsuki, H. Kusunose, P. Werner, and Y. Kuramoto, *J. Phys. Soc. Jpn.* **76**, 114707 (2007).
¹¹J. Otsuki, H. Kusunose, and Y. Kuramoto, *J. Phys. Soc. Jpn.* **78**, 014702 (2009).
¹²J. Otsuki, H. Kusunose, and Y. Kuramoto, *J. Phys. Soc. Jpn.* **78**, 034719 (2009).
¹³B. Coqblin and J. R. Schrieffer, *Phys. Rev.* **185**, 847 (1969).
¹⁴H. J. Vidberg and J. W. Serene, *J. Low Temp. Phys.* **29**, 179 (1977).
¹⁵U. Fano, *Phys. Rev.* **124**, 1866 (1961).
¹⁶G. D. Mahan, *Many-Particle Physics*, 3rd ed. (Plenum, New York, 2000).
¹⁷A. C. Hewson, *The Kondo Problem to Heavy Fermions* (Cambridge University Press, Cambridge, 1993).
¹⁸C. Grenzbach, F. B. Anders, G. Czycholl, and T. Pruschke, *Phys. Rev. B* **74**, 195119 (2006).
¹⁹D. R. Hamann, *Phys. Rev.* **158**, 570 (1967).
²⁰P. Nozières, *J. Low Temp. Phys.* **17**, 31 (1974).
²¹A. Houghton, N. Read, and H. Won, *Phys. Rev. B* **35**, 5123 (1987).
²²The S matrix is given by $S = T_{\tau} \exp[\int_{-\infty}^{\infty} H_{\text{int}}(\tau) d\tau]$ in the interaction representation, where T_{τ} is the time-ordering operator with τ being the imaginary time.
²³G. Zaránd, L. Borda, J. von Delft, and N. Andrei, *Phys. Rev. Lett.* **93**, 107204 (2004).
²⁴L. Borda, L. Fritz, N. Andrei, and G. Zaránd, *Phys. Rev. B* **75**, 235112 (2007).